2019

Go@Se@ni cathode materials for lithium-selenium battery

Jun Liu
Guangdong University of Technology

Daoyun Lan
Guangdong University of Technology

Xinyue Huang
Guangdong University of Technology

Feitao Zhang
Guangdong University of Technology

Aiqi Huang
Guangdong University of Technology

See next page for additional authors

Go@Se@ni cathode materials for lithium-selenium battery

Abstract

Selenium is a promising cathode material for high-energy lithium batteries. In this work, selenium was electrodeposited on nickel foam from aqueous selenite solution. The influences of pH values and current density on electrodeposited Se@Ni were investigated. It is found that electrodeposition at pH 7 and 0.5 mA cm −2 enables high current efficiency and produces uniform and smooth deposits. Graphene oxide (GO) was further coated on Se@Ni through physical adsorption to produce GO@Se@Ni. The developed GO@Se@Ni electrode delivers a high initial specific capacity of 593 mAh g −1 and good capacity retention over 100 cycles at 0.1 C.

Disciplines

Engineering | Science and Technology Studies

Publication Details

Liu, J., Lan, D., Huang, X., Zhang, F., Huang, A., Xiao, Y., Zhao, Z., Liu, L., Ke, X., Shi, Z. & Guo, Z. (2019). Go@Se@ni cathode materials for lithium-selenium battery. Journal of the Electrochemical Society, 166 (3), A5259-A5264.

Authors

Jun Liu, Daoyun Lan, Xinyue Huang, Feitao Zhang, Aiqi Huang, Yaoxin Xiao, Zhuozhuo Zhao, Liying Liu, Xi Ke, Zhicong Shi, and Zaiping Guo

JES Focus Issue of Selected Papers from IMLB 2018

GO@Se@Ni Cathode Materials for Lithium-Selenium Battery

Jun Liu,[1] Daoyun Lan,[1] Xinyue Huang,[1] Feitao Zhang,[1] Aiqi Huang,[1] Yaoxin Xiao,[1] Zhuozhuo Zhao,[1] Liying Liu,[1] Xi Ke,[1] Zhicong Shi,[1,z] and Zaiping Guo[1,2,z]

[1]*Guangdong Provincial Engineering Technology Research Centre for New Energy Materials and Devices, School of Materials and Energy, Guangdong University of Technology, Guangzhou, 510000, People's Republic of China*
[2]*School of Mechanical, Materials, and Mechatronic Engineering, Institute for Superconducting & Electronic Materials, Faculty of Engineering, University of Wollongong, Wollongong, NSW 2522, Australia*

Selenium is a promising cathode material for high-energy lithium batteries. In this work, selenium was electrodeposited on nickel foam from aqueous selenite solution. The influences of pH values and current density on electrodeposited Se@Ni were investigated. It is found that electrodeposition at pH 7 and 0.5 mA cm^{-2} enables high current efficiency and produces uniform and smooth deposits. Graphene oxide (GO) was further coated on Se@Ni through physical adsorption to produce GO@Se@Ni. The developed GO@Se@Ni electrode delivers a high initial specific capacity of 593 mAh g^{-1} and good capacity retention over 100 cycles at 0.1 C.
 [DOI: 10.1149/2.0411903jes]

Manuscript submitted October 23, 2018; revised manuscript received November 26, 2018. Published December 29, 2018. *This paper is part of the JES Focus Issue of Selected Papers from IMLB 2018.*

Current lithium-ion (Li-ion) batteries with transition-metal oxide/phosphate cathodes and graphite anode are insufficient to satisfy the crucial demand of electric vehicles and smart grid energy stations. Some efforts have been done to replace carbon anode with high capacity materials such as silicon,[1] tin[2] and recent lithium metal.[3–5] However, the development of high-capacity cathode materials is more urgently needed because the energy density of commercial Li-ion batteries is mainly limited by the cathode materials.[6]

Beyond conventional intercalation chemistry, the multi-electron conversion reaction of lithium with oxygen,[7] sulfur[8,9] and selenium[10–12] have the potential to provide much higher energy density. Following the widely studied lithium–sulfur and lithium-oxygen systems, selenium (Se) has gained significant attentions due to its high theoretical capacity of 675 mAh g^{-1}, which is much higher than commercial cathodes with typical capacities of 120 - 200 mAh g^{-1}.[13] In addition, selenium also has other two promising properties: high electronic conductivity (1×10^{-3} S m^{-1}) and high theoretical volumetric capacity density (3253 Ah L^{-1}).[14] Bearing in mind that battery packs for commercial applications shall be installed in limited space, the high theoretical volumetric capacity of Se is favorable.

Selenium faces the dissolution issue of intermediary polyselenide species during cycling, which usually results in fast capacity fading and low coulombic efficiency. The common strategy is to encapsulate Se with porous carbon.[15–17] Although carbon host can inhibit the dissolution of polyselenides into electrolyte, it unavoidably reduces the energy density of whole cathode.

Here, we proposed to prepare selenium cathode via electrodeposition in order to avoid a lot of carbon additives. Meanwhile, electrodeposition allows direct deposition of active materials onto conducting substrates, enabling binder-free fabrication. The elimination of binder not only saves cost, but also avoids related environmental problem associated with the evaporation of organic solvent during the process of electrode fabrication. With this merit, electrodeposition has been used to prepare anode materials such as Si composite[18] and tin compound.[2] In order to alleviate the dissolution of polyselenides, a thin layer of GO was introduced as physical barrier on the surface of electrodeposited Se via simple physical adsorption.

Experimental

Preparation of Se@Ni cathodes.—The electrodeposition was performed using a CHI750 electrochemical workstation (Shanghai Chenhua) in a glass beaker at room temperature with a three-electrode cell configuration: nickel (Ni) foam (thickness 0.5 mm, area 1 × 1 cm^2) as the working electrode, titanium mesh as the counter electrode, saturated calomel electrode (SCE) as the reference electrode.

Ni foam substrates were sequentially treated with acetone, alcohol, deionized water and 3.0 M hydrochloric acid for 10 min in an ultrasonic bath before use. Titanium mesh was ultrasonically rinsed with 50 wt% nitric acid solution and then washed with deionized water.

The electroplating bath contains 0.1 M selenium oxide (SeO_2) and 0.25 M potassium chloride. The pH values of electroplating solutions were adjusted by addition of potassium hydroxide. Potentiostatic electrodeposition (−0.6 V vs. SCE) was only applied to investigate the influence of different pH values (2.5, 4, 7). Other samples were prepared by galvanostatic electrodeposition. Three different currents (0.5, 1 and 2 mA) were investigated on the 1 × 1 cm^2 Ni foam. The mass of deposited Se at 0.5 mA for 3h was about 1.0 mg.

Preparation of GO@Se@Ni cathodes.—GO powders were ultrasonically dispersed in deionized water to make a suspension (0.2 mg ml^{-1}). Se@Ni cathodes were dipped into the GO solution for 1 minute, and then dried under vacuum. This dip-drying process was repeated three times to obtain GO@Se@Ni cathodes. The content of GO in the composite electrode is 0.05 - 0.1 mg.

Electrochemical measurements.—Se@Ni and GO@Se@Ni were used directly as cathodes to fabricate CR2032-type coin cells with lithium foil as the counter electrode and polypropylene microporous sheet (Celgard 2300) as the separator. The electrolyte is 1.0 M lithiumbis(trifluoromethanesulfonyl)imide (LiTFSI) in 1,3-dioxolane(DOL) and 1,2-dimethoxyethane (DME) (volume ratio 1:1) with 1.0 wt% $LiNO_3$ additive. 0.1 ml electrolyte was used in a coin cell. The assembled cells were galvanostatically cycled between 1.5 and 3.0 V at different current rates using a battery tester (Neware SBT7.5). Cyclic voltammetry (CV) measurement was conducted using CHI750 electrochemical workstation at 0.1 mV s^{-1} in the voltage range from 1.2 to 3.0 V.

Characterization.—The morphologies of prepared cathodes were characterized using a scanning electron microscope (SEM, Hitachi SU8010). The crystal structures of cathodes were analyzed by X-ray diffraction (XRD, Rigaku D/max-2200/PC). The chemical properties of cathodes were characterized by Raman scattering spectra (INVIA, λ = 532 nm).

[z]E-mail: zhicong@gdut.edu.cn; zguo@uow.edu.au

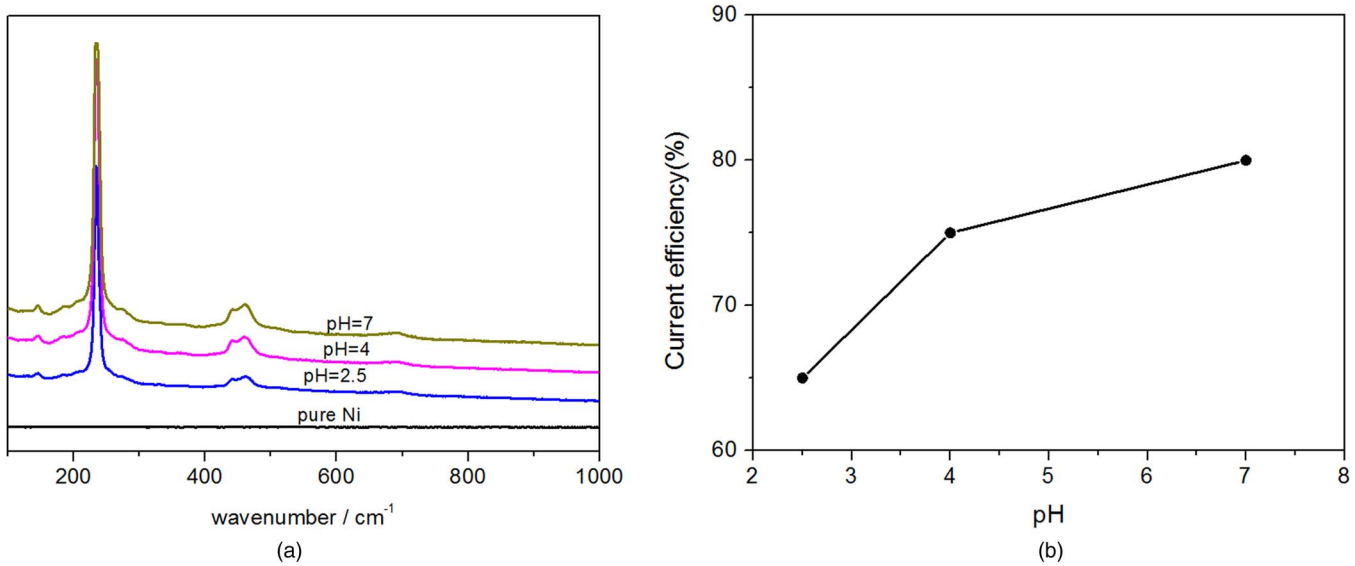

Figure 1. (a) Raman spectra and (b) current efficiency for the deposited Se at different pH values. (Electrodeposition potential −0.6 V vs. SCE and time 0.5 h).

Results and Discussion

The reduction of selenite to selenium involves several different reactions. According to the potential-pH diagram for the system selenium-water at 25°C,[19,20] at lower pH value, selenite is reduced to Se at higher potential; meanwhile Se also tends to be reduced to H_2Se or HSe^- at higher potential. This means that at low pH value Se is not only more easily to form, but also more vulnerable to be transferred to soluble H_2Se. Therefore, three different pH values (2.5, 4 and 7) were investigated for electrodeposition. Following the potential-pH diagram, potentiostatic electrodeposition (−0.6 V vs. SCE) was applied. Figure 1a shows the Raman spectroscopy for the deposited Se at different pH values. All samples display three peaks at 142, 235, and 460 cm^{-1}, respectively. The sharp peak at 235 cm^{-1} represents chain-structure Se molecule, while the peaks at 142 and 460 cm^{-1} are attributed to Se_{12} with a ring structure.[21,22] The Raman spectroscopies for three samples are similar, indicating that compositions of deposited Se at different pH values are the same.

Figure 1b shows the current efficiency of electrodeposition at different pH values. The real mass of deposits was divided by the theoretical mass calculated from electric quantity to obtain the current efficiency. Sample prepared at pH 2.5 shows only 65% current efficiency. The current efficiency increases to 75% as the pH is increased to 4. While at pH 7 it shows the highest current efficiency of 80%. These results indicate that at low pH value there are more side reactions during the electrodepositing process.

Figure 2 presents the typical SEM images of pure Ni foam and deposited Se at different pH values. Ni foam has a smooth surface with regular cracks, as shown in Fig. 2a. The deposits at pH 2.5 are isolated particles (Fig. 2b). At pH 4, the density of particles increases and particles grow up (Fig. 2c). At pH 7, as seen in Fig. 2d, the whole surface is covered with particles and cracks of Ni surface are no longer observed. The SEM images prove that more deposits are prepared at higher pH value, which is consistent with the current efficiency.

Figure 3a shows the CV of coin cell using deposited Se at pH 7 as cathode. The CV measurements are initiated with a lithiation process by negative scan from the open-circuit voltage. During the first cathodic scans, two wide peaks are observed at about 1.9 and 1.65 V, which correspond to the stepwise reduction of Se to polyselenides, and polyselenides to Li_2Se, respectively.[23] At the first anodic scan, a sharp peak is observed at 2.25 V. During the second and third CVs, all cathodic and anodic peaks shift positively. This phenomenon is ascribed to the generation of soluble polyselenide ions in the first cycle, which facilitate the electrochemical reactions in the following cycles. Fig. 3b displays the charge-discharge profile of the deposited Se at pH 7. Two discharge plateaus (2.16 V and 1.99 V) and one long charge plateau (2.2 V) are observed. The discharge and charge capacities decrease gradually with cycles. This capacity fading upon long cycling is mainly attributed to the dissolution of polyselenides into electrolyte. The cycle performance of the deposited Se at different pH values are shown in Fig. 3c. Sample prepared at pH = 2.5 shows higher capacity and slower capacity decay than pH 4 and 7 only for the first 20 cycles. As mentioned above, due to serious side reactions and low current efficiency of 65% during the electrodeposition, sample pH 2.5 has the smallest particle size and lowest mass loading, which facilitate the electrochemical reaction and bring better performance at the beginning stage. As the cycles are going on, the influence of polyselenides dissolution on low mass-loading sample becomes more prominent, resulting in faster capacity decay. Compared to pH 2.5 and 4, pH 7 exhibits less pronounced capacity fading over 100 cycles. The improved capacity retention at pH 7 is ascribed to its high mass loading and unique morphology, which is compact and uniformly distributed.

Figure 4 exhibits the typical SEM images of deposited Se at different current densities. At current density of 0.5 mA cm^{-2}, the deposits

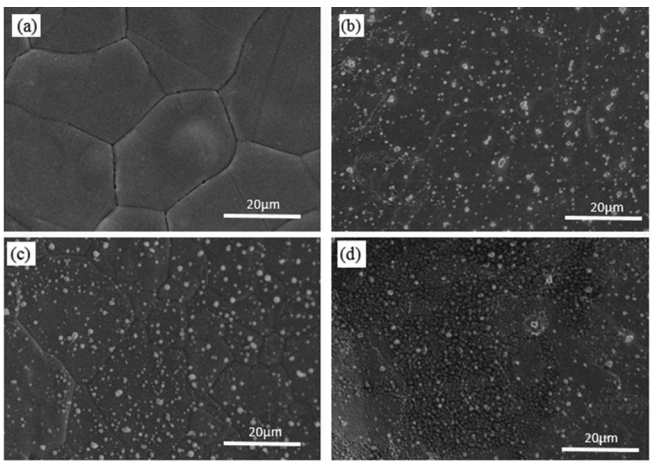

Figure 2. Typical SEM images: (a) pure Ni foam and deposited Se at different pH values: (b) pH = 2.5, (c) pH = 4, (d) pH = 7.

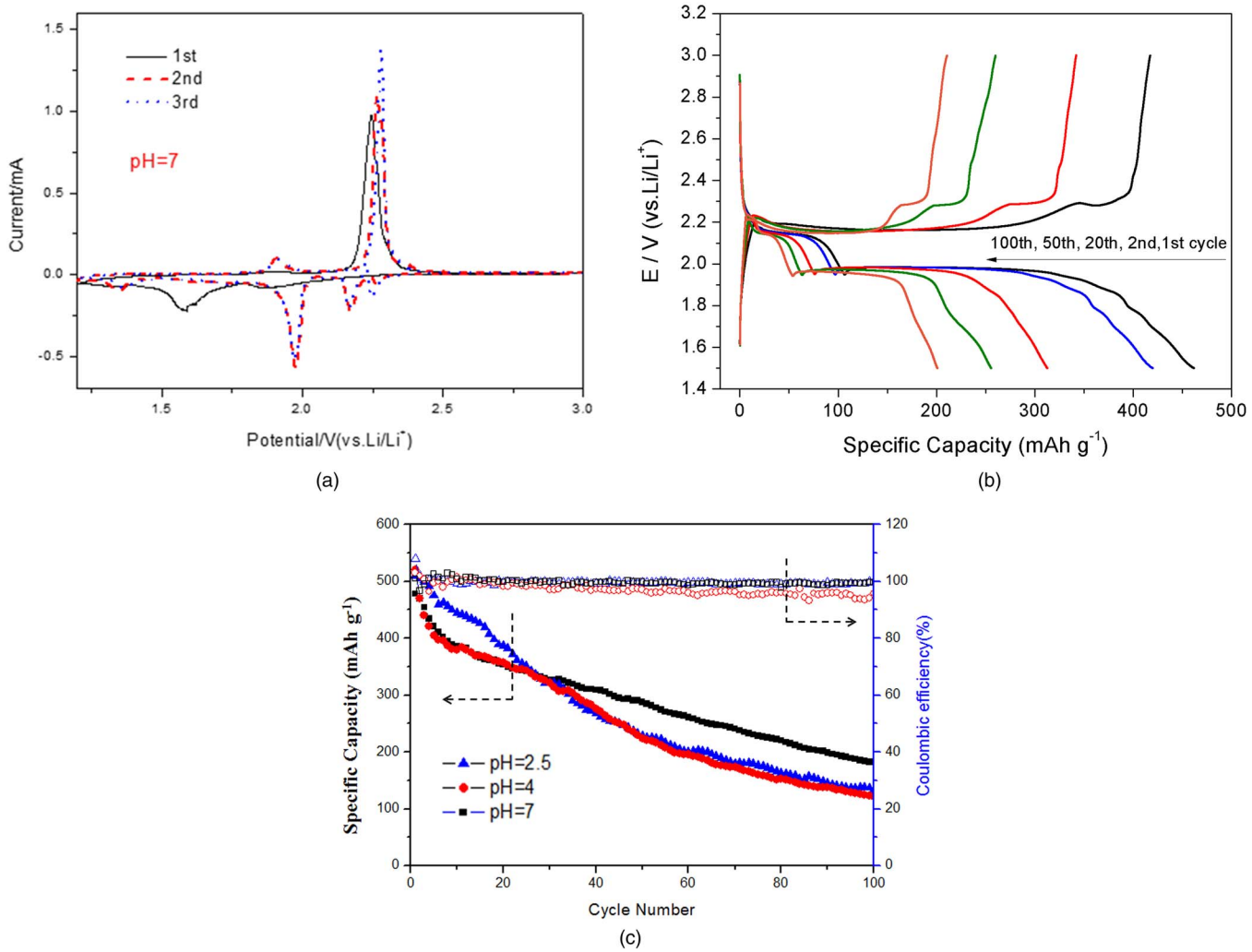

Figure 3. (a) Cyclic voltammograms of coin cell using deposited Se at pH = 7; (b) the galvanostatic discharge/charge profiles of deposited Se at pH = 7 at 0.1 C; (c) Cycling performance and coulombic efficiency of deposited Se at different pH values. (Electrodeposition potential −0.6 V vs. SCE and time 0.5 h).

are uniformly distributed balls, as shown in Fig. 4a. When current of 1 mA was applied, the spherical particles grow up and in some area rod-like big particles form (Fig. 4b). At high current density of 2 mA cm^{-2}, large bulk deposits full of cracks are observed on the surface, as seen in Fig. 4c. This bulk Se easily peels off even during the washing and drying process. Fig. 4d shows the EDX spectrum of the deposited Se at 0.5 mA cm^{-2}, which contains element Se, Ni and O. The element O may come from the surface oxidization of Ni foam. Elemental mapping of Ni and Se are displayed in Figs. 4e and 4f, respectively. It clearly reveals a uniform distribution of Se among the Ni substrate surface.

Figure 5a shows the current efficiency of electrodeposition for 1h at different current conditions. Higher current density obviously produces more deposits, but at the expense of efficiency. At 2 mA cm^{-2}, the current efficiency is only 52% possibly because more side reactions such as the production of soluble H_2Se and evolution of hydrogen occur under high polarization. Although 0.5 mA cm^{-2} has high efficiency of 80%, the mass of deposits is low, which agrees with the observation of SEM images. The chemical compositions of deposited Se at different current densities were examined by Raman spectroscopy (Fig. 5b). All samples display similar peaks at 142, 235, and 460 cm^{-1}, which indicates that the compositions of deposited Se at different current densities are the same.

The cycle performances of coin cells using deposited Se at different current densities are shown in Fig. 5c. At 0.1 C a high discharge capacity of 560 mAh g^{-1} was obtained at the 1st cycle for both samples. The 0.5 mA cm^{-2} sample shows higher capability of capacity retention possibly due to lower mass of active materials. The average coulombic efficiencies for both samples were 98% during 100 cycles. At 0.5 C (Fig. 5d), the 0.5 mA cm^{-2} sample also exhibits better capacity retention than 1 mA cm^{-2}. However, both samples show fast capacity fading in the first 50 cycles.

Figure 6a presents surface morphology of Se@Ni prepared at 0.5 mA cm^{-2} for 3 h. The surface of Se@Ni is full of tiny spherical particles. GO@Se@Ni shows a similar morphology (Fig. 6b). And a thin film with wrinkles, as typical morphology of graphene oxide, is covered on the surface of deposits. XRD was used to characterize the structures of samples, as shown in Fig. 6c. Only peaks of Ni substrate are observed in Se@Ni, which means that the deposited Se is amorphous. For GO@Se@Ni, a small peak was observed at 27°, which is assigned to the GO. Fig 6d demonstrates the Raman spectroscopy for Se@Ni and GO@Se@Ni. Both samples display a sharp peak at 235 cm^{-1} and a small peak at 460 cm^{-1}, which are the typical feature of Se as mentioned above. Two strong peaks at 1354 and 1595 cm^{-1} are distinguished in GO@Se@Ni, which represent the D and G bands of graphene oxide, respectively.[24] The Raman spectra real that GO is physically adsorbed on the surface of Se@Ni.

Figure 7a shows the Nyquist plots for Se@Ni and GO@Se@Ni, which are composed of one depressed semicircle in the high frequency region and one straight line in the low frequency region. The charge

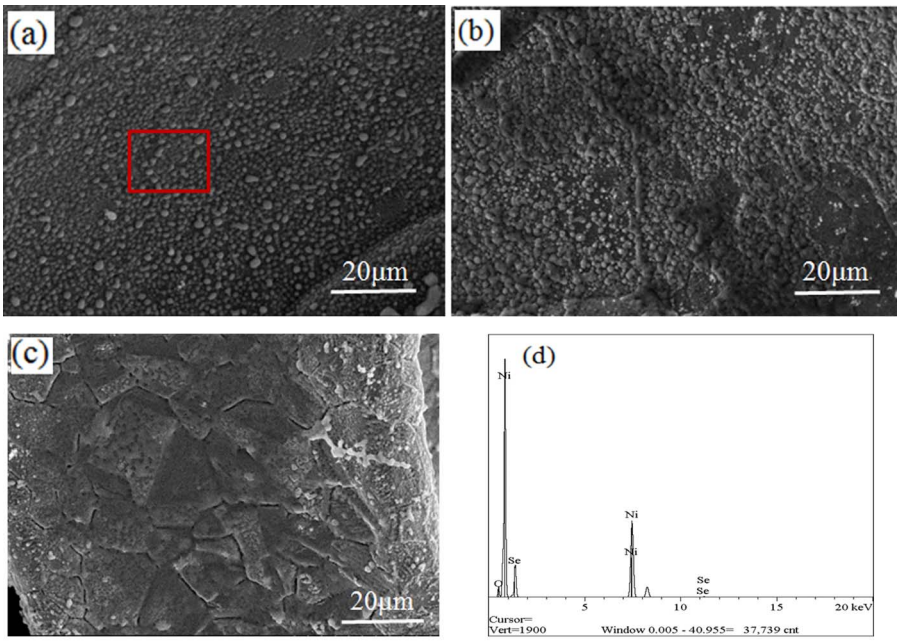

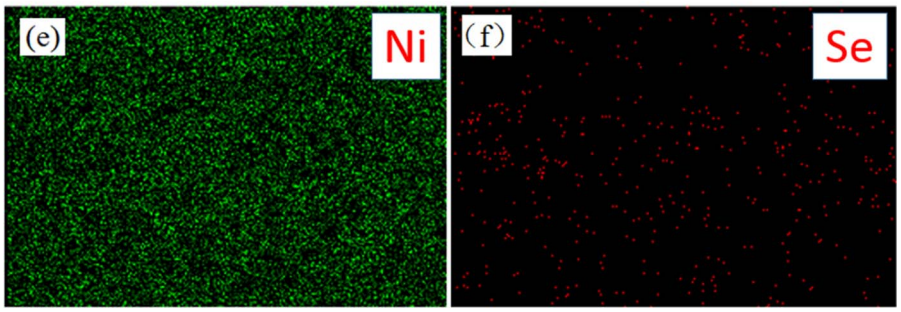

Figure 4. SEM images of Se@Ni electrodeposited at different currents with 1 × 1 cm^2 Ni foam substrates (electrodeposition time 1 h at pH = 7): (a) 0.5 mA; (b) 1 mA; (c) 2 mA. (d) EDX spectrum of Se@Ni prepared at 0.5 mA (detection area is as marked by red rectangle in Fig. 4a). Elemental mapping for Se@Ni prepared at 0.5 mA: (e) nickel; (f) selenium.

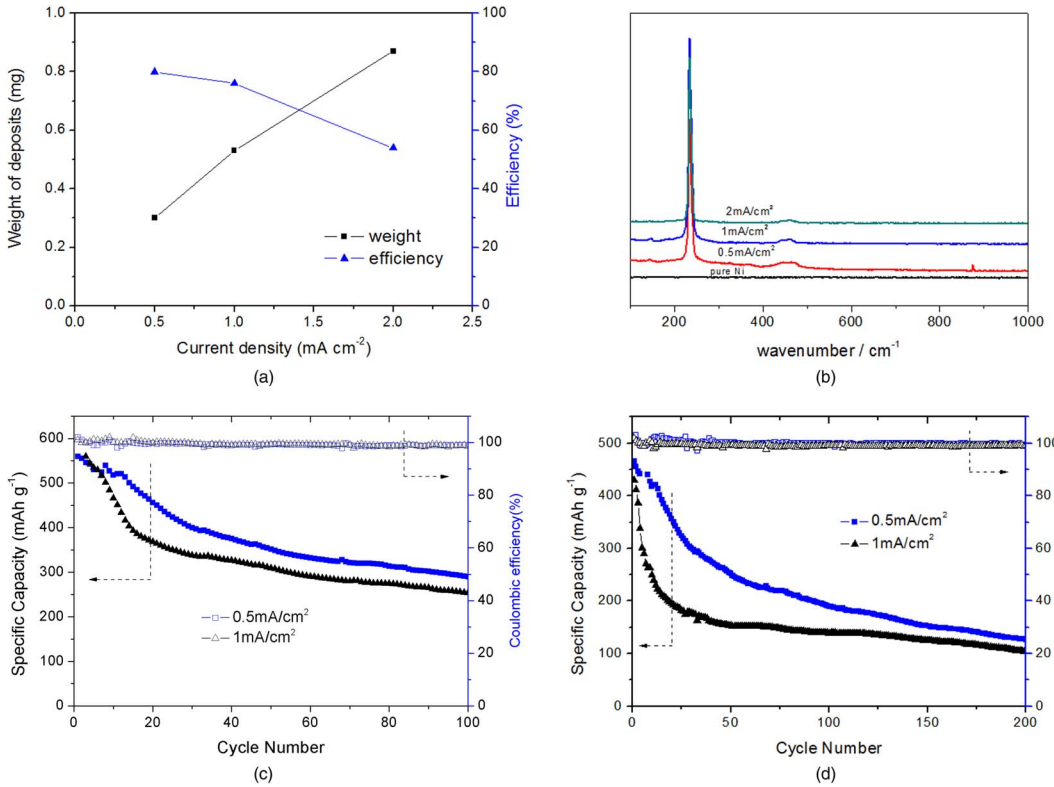

Figure 5. (a) Change of deposit weight and current efficiency with applied current density; (b) Raman spectra. Cycling performance and coulombic efficiency for Se@Ni at different C rates: (c) 0.1 C; (d) 0.5 C. Se@Ni were electrodeposited with various current densities for 1 h at pH = 7.

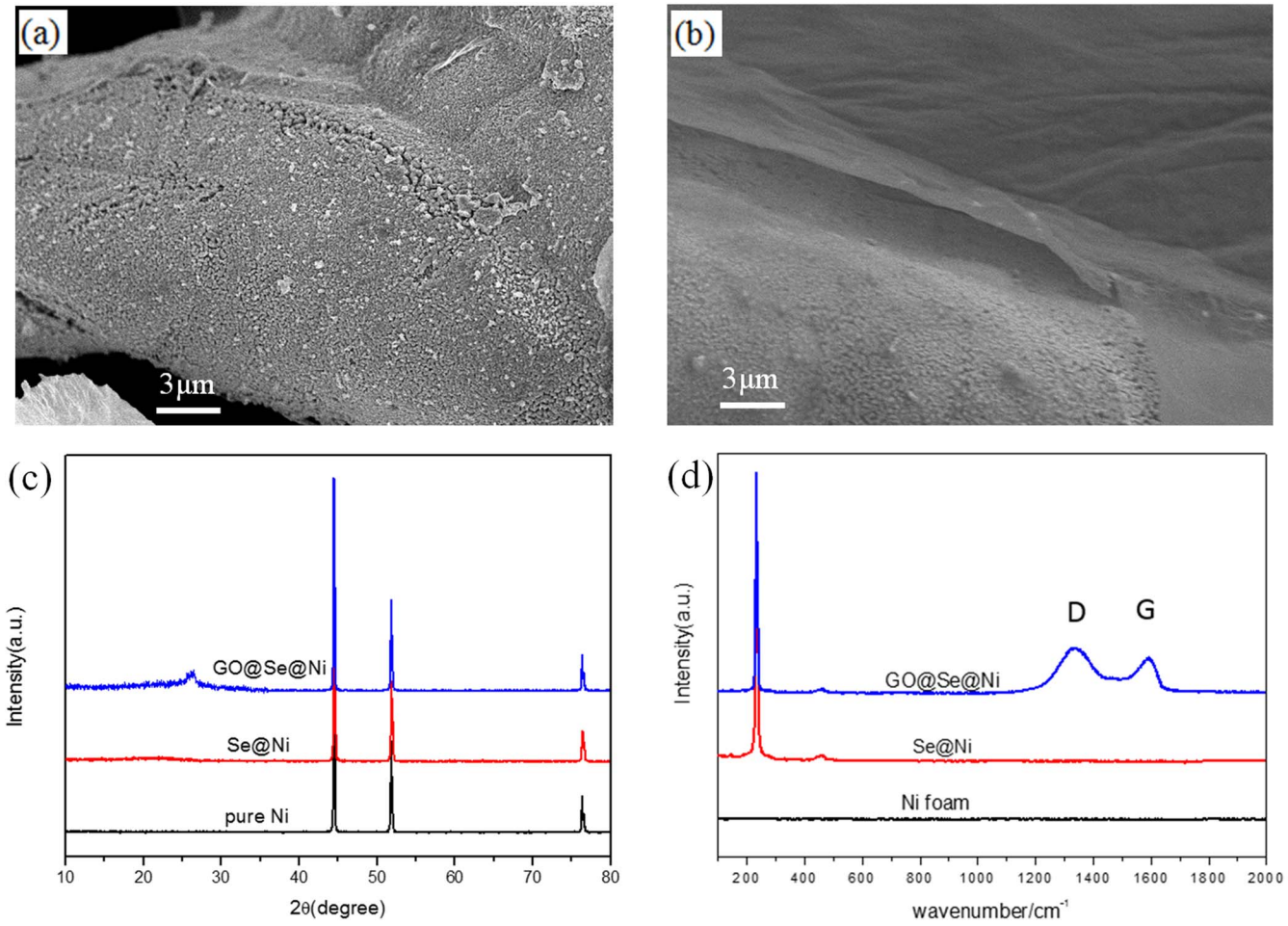

Figure 6. SEM images for: (a) Se@Ni; (b) GO@Se@Ni. (c) XRD patterns; (b) Raman spectra. The electrodeposition condition for Se@Ni preparation was 0.5 mA with 1 × 1 cm^2 Ni foam for 3 h at pH = 7.

transfer resistance at the interface of GO@Se@Ni is smaller than Se@Ni, indicating that GO facilitates the charge transfer process. The cycle performances at 0.1 C are demonstrated in Fig. 7b. Se@Ni prepared by electrodeposition for 3 h seems to have inferior capacity retention than the sample electrodeposited for 1 h (Fig. 5c). As the mass of active materials increases, usually the utilization of active materials decreases, resulting in worse cycle performance.[25] Thus, the increase of electrodeposition time produces more deposits and makes the battery performance worse. Thanks to the help of GO, GO@Se@Ni exhibit better capacity retention than Se@Ni. GO works as physical barrier and adsorption site to trap polyselenides and inhibit their dissolution. Because physically adsorbed GO does not cover all

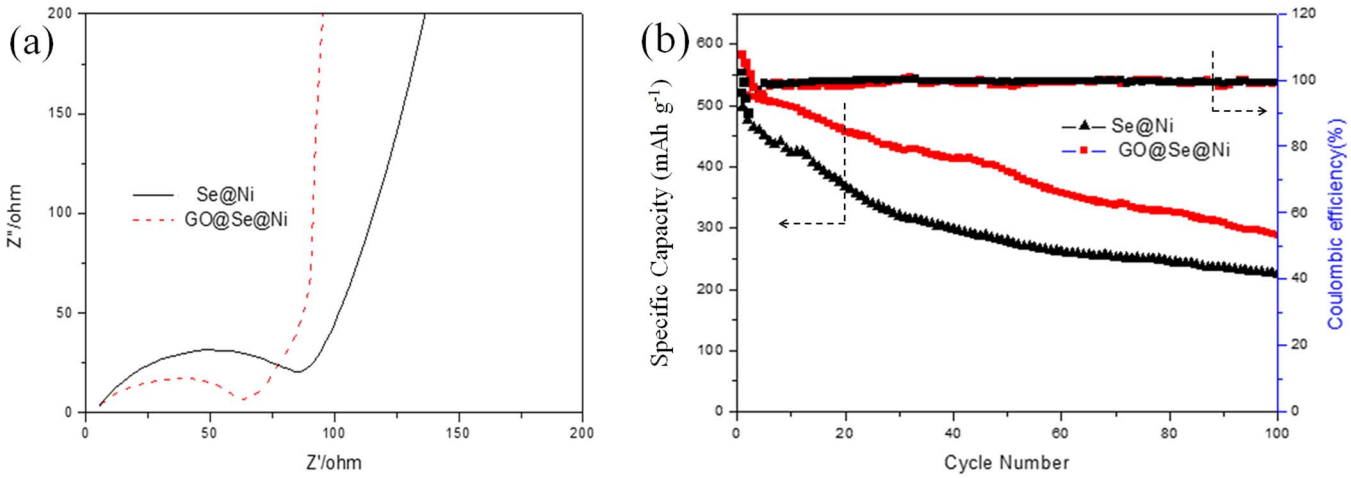

Figure 7. Electrochemical performances: (a) impedance spectra; (b) capacity retention at 0.1 C. The electrodeposition condition for Se@Ni preparation was 0.5 mA with 1 × 1 cm^2 Ni foam for 3 h at pH = 7.

the surface of deposited Se, as shown above in Fig. 6b, polyselenides can still dissolve into electrolyte through uncovered area, resulting in considerable capacity fading in GO@Se@Ni.

Conclusions

Electrodeposition in aqueous selenite solution was used to fabricate Se@Ni cathodes. The pH value of electroplating solutions and applied current strongly influence the morphology and performance of deposits. High current efficiency, uniform and smooth deposits were obtained at the condition of pH 7 and 0.5 mA cm^{-2}. Finally, GO was introduced as spatial restriction on the surface of Se@Ni via simple physical adsorption. The prepared GO@Se@Ni delivers a high initial capacity of 593 mAh g^{-1} and shows good cycling behavior. This method is simple and easy to scale up. It does not need binder, conductive agent and organic solvent to make slurry and coating. This fabrication based on electrodeposition can be further extended to other conductive substrate and flexible batteries for soft portable electronic devices.

Acknowledgments

The work was supported by the National Natural Science Foundation of China (NNSFC 51604086, 21673051), the Guangzhou Science & Innovative Committee (201704030011).

ORCID

Jun Liu https://orcid.org/0000-0002-1920-2927
Liying Liu https://orcid.org/0000-0002-5447-774X
Zhicong Shi https://orcid.org/0000-0003-2360-7668

References

1. C. K. Chan, H. Peng, G. Liu, K. McIlwrath, X. F. Zhang, R. A. Huggins, and Y. Cui, *Nat. Nanotech.*, **3**, 31 (2007).
2. M. Jeong, T. Yokoshima, H. Nara, T. Momma, and T. Osaka, *J. Electrochem. Soc.*, **161**, D3025 (2014).
3. M. Bai, K. Xie, K. Yuan, K. Zhang, N. Li, C. Shen, Y. Lai, R. Vajtai, P. Ajayan, and B. Wei, *Adv. Mater.*, **30**, 1801213 (2018).
4. N. Li, W. Wei, K. Xie, J. Tan, L. Zhang, X. Luo, K. Yuan, Q. Song, H. Li, C. Shen, E. M. Ryan, L. Liu, and B. Wei, *Nano Lett.*, **18**, 2067 (2018).
5. X. Ke, Y. Cheng, J. Liu, L. Liu, N. Wang, J. Liu, C. Zhi, Z. Shi, and Z. Guo, *ACS Appl. Mater. Interfaces*, **10**, 13552 (2018).
6. A. Manthiram, *ACS Central Science*, **3**, 1063 (2017).
7. Z. Peng, S. A. Freunberger, Y. Chen, and P. G. Bruce, *Science*, **337**, 563 (2012).
8. H. Nara, T. Yokoshima, H. Mikuriya, S. Tsuda, T. Momma, and T. Osaka, *J. Electrochem. Soc.*, **164**, A5026 (2017).
9. K. Xie, Y. You, K. Yuan, W. Lu, K. Zhang, F. Xu, M. Ye, S. Ke, C. Shen, X. Zeng, X. Fan, and B. Wei, *Adv. Mater.*, **29**, 1604724 (2017).
10. A. Abouimrane, D. Dambournet, K. W. Chapman, P. J. Chupas, W. Weng, and K. Amine, *J. Am. Chem. Soc.*, **134**, 4505 (2012).
11. C.-P. Yang, S. Xin, Y.-X. Yin, H. Ye, J. Zhang, and Y.-G. Guo, *Angew. Chem. Int. Ed.*, **125**, 8521 (2013).
12. J. Guo, Q. Wang, J. Jin, C. Chen, and Z. Wen, *J. Electrochem. Soc.*, **163**, A654 (2016).
13. J. G. Siqi Shi, Yue Liu, Yan Zhao, Qu Wu, Wangwei Ju, Chuying Ouyang, and Ruijuan Xiao, *Chin. Phys. B*, **25**, 018212 (2016).
14. L. Zeng, W. Zeng, Y. Jiang, X. Wei, W. Li, C. Yang, Y. Zhu, and Y. Yu, *Adv. Energy Mater.*, **5**, 1401377 (2015).
15. Z. Li, L. Yuan, Z. Yi, Y. Liu, and Y. Huang, *Nano Energy*, **9**, 229 (2014).
16. J. T. Lee, H. Kim, M. Oschatz, D.-C. Lee, F. Wu, H.-T. Lin, B. Zdyrko, W. I. Cho, S. Kaskel, and G. Yushin, *Adv. Energy Mater.*, **5**, 1400981 (2015).
17. J. Zhang, Z. Zhang, Q. Li, Y. Qu, and S. Jiang, *J. Electrochem. Soc.*, **161**, A2093 (2014).
18. T. Momma, S. Aoki, H. Nara, T. Yokoshima, and T. Osaka, *Electrochem. Commun.*, **13**, 969 (2011).
19. M. Bouroushian, Electrochemistry of Metal Chalcogenides, 2010, XII, 358 p. 69 illus.
20. Y. Lai, C. Han, C. Yan, F. Liu, J. Li, and Y. Liu, *J. Alloys Compd.*, **557**, 40 (2013).
21. C. Luo, Y. Xu, Y. Zhu, Y. Liu, S. Zheng, Y. Liu, A. Langrock, and C. Wang, *ACS Nano*, **7**, 8003 (2013).
22. R. Lukacs, M. Veres, K. Shimakawa, and S. Kugler, *J. Appl. Phys.*, **107**, 073517 (2010).
23. Y. Cui, A. Abouimrane, J. Lu, T. Bolin, Y. Ren, W. Weng, C. Sun, V. A. Maroni, S. M. Heald, and K. Amine, *J. Am. Chem. Soc.*, **135**, 8047 (2013).
24. K. Han, Z. Liu, H. Ye, and F. Dai, *J. Power Sources*, **263**, 85 (2014).
25. C. Wu, L. Yuan, Z. Li, Z. Yi, R. Zeng, Y. Li, and Y. Huang, *Science China Materials*, **58**, 91 (2015).